Available online at www.sciencedirect.com

SciVerse ScienceDirect

Advances in Space Research 51 (2013) 1834–1841

ADVANCES IN SPACE RESEARCH (a COSPAR publication)

www.elsevier.com/locate/asr

Study of magnetic flux emergence and related activity in active region NOAA 10314

Mariano Poisson [a,b], Marcelo López Fuentes [a,b,*], Cristina H. Mandrini [a,b], Pascal Démoulin [c], Etienne Pariat [c]

[a] Instituto de Astronomía y Física del Espacio (CONICET-UBA), CC 67 Suc 28, 1428 Buenos Aires, Argentina
[b] Facultad de Ciencias Exactas y Naturales, UBA, Buenos Aires, Argentina
[c] Observatoire de Paris, LESIA, Observatoire de Paris, CNRS, UPMC, Universit Paris Diderot, 92190 Meudon, France

Available online 15 March 2012

Abstract

We study the extremely complex active region (AR) NOAA 10314, that was observed from March 13–19, 2003. This AR was the source of several energetic events, among them two major (X class) flares, along a few days. We follow the evolution of this AR since the very first stages of its emergence. From the photospheric evolution of the magnetic polarities observed with SOHO/MDI we infer the morphology of the flux tube that originates the AR. Using a computation technique that combines Local Correlation Tracking with magnetic induction constrains, we compute the rate of magnetic helicity injection at the photosphere during the observed evolution. From our results we conclude that the AR originated by the emergence of a severely deformed magnetic flux tube having a dominantly positive magnetic helicity.

Keywords: Solar active regions; Magnetic flux emergence; Magnetic helicity injection

1. Introduction

It is widely recognized that magnetically complex solar active regions (ARs) are the most productive in terms of number and intensity of flares and coronal mass ejections (CMEs) (Liu et al., 2005). In this context magnetic complexity means distribution of photospheric magnetic flux that departs from the usual bipolar configuration expected according to Hale's law (Hale and Nicholson, 1938). ARs with magnetic flux distributions that form δ-spots at the photospheric level are among these cases. This kind of structures are generally interpreted as the emergence of magnetic flux tubes that have been distorted from the normal Ω-loop shape, commonly associated to bipolar ARs (Schrijver and Zwaan, 2000, Chapter 5).

The axis of the magnetic bipoles that form normal ARs tend to have a small inclination, called tilt angle, with respect to the east–west direction. This characteristic of the ARs is known as the Joy's law (Hale et al., 1919). The presence of a tilt angle is thought to be due to the Coriolis force acting on the emerging flux tubes (D'Silva and Choudhuri, 1993) and the observed statistical dispersion around the mean has been associated to the buffeting produced by turbulence in the convection zone (Longcope and Choudhuri, 2002).

Although the origin of extreme flux tube deformations is still a matter of investigation (Fan, 2009), both observations and models agree that the magnetic structures, that form peculiarly complex ARs, emerge torsionally stressed and with high contents of magnetic helicity. These emerging sheared fields inject and accumulate in the solar

* Corresponding author at: Instituto de Astronomía y Física del Espacio (CONICET-UBA), CC 67 Suc 28, 1428 Buenos Aires, Argentina. Tel.: +54 11 4781 6755; fax: +54 11 4786 8114.
E-mail addresses: marianopoisson@gmail.com (M. Poisson), lopezf@iafe.uba.ar (M. López Fuentes), mandrini@iafe.uba.ar (C.H. Mandrini), Pascal.Demoulin@obspm.fr (P. Démoulin), etienne.pariat@obspm.fr (E. Pariat).

0273-1177/$36.00 © 2012 COSPAR. Published by Elsevier Ltd. All rights reserved.
doi:10.1016/j.asr.2012.03.010

atmosphere large amounts of free magnetic energy that is released, under the proper conditions, by reconnection, restructuring of the field, and eventually ejecting matter and magnetic structures to interplanetary space.

Here, we study AR NOAA 10314, observed from emergence on March 13, 2003 to disappearance on the West limb around March 20, 2003 (see Morita and McIntosh, 2005). At the maximum of its magnetic strength this AR presented a complex quadrupolar configuration with a δ-spot in its central region. In Section 2 we describe the observed photospheric and coronal evolution of the AR and the production of a series of very intense flares. In Section 3 we compute and analyze the evolution of the tilt angle of the δ-spot and the magnetic helicity injected in the AR. In Section 4 we discuss and interpret the studied evolution in terms of the emergence of a very distorted magnetic flux tube. We present our concluding remarks in Section 5.

2. Description of the observations

2.1. AR 10314 photospheric evolution

To study the photospheric magnetic evolution of AR 10314 we used a set of 163 full disk longitudinal magnetograms taken with the Michelson Doppler Imager (MDI, Scherrer et al., 1995) on board the Solar and Heliospheric Observatory (SOHO), between March 13 and 19, 2003. The time between two consecutive magnetograms is 96 min. In Fig. 1 we present a subset of magnetograms showing the AR for selected dates during the studied evolution. The first emergence of the AR occurs close to the east side of the central meridian (~E15 S15). It begins with the appearance of a series of small bipoles that rapidly coalesce to form two larger bipolar structures that we identify with the labels E1 and E2 in Fig. 1 upper left panel. The indexes (1 and 2) indicate the order of formation of the bipoles. Both of them have negative preceding polarities corresponding to the expected orientation according to Hale's law for Solar Cycle 23. By March 14 and 15 emergence continues and the positive polarity of E1 and the negative polarity of E2 pack together to form a δ-spot observed in white light. In the central left panel of Fig. 1 we indicate the area corresponding to the δ configuration. The δ-spot continues to be present during the full observed evolution of the AR. A feature that is of particular interest in this work is the constant rotation of the inversion line of the δ-spot (see panels 3–6 in Fig. 1).

In Fig. 2 we plot the magnetic flux of the positive and negative polarities of bipoles E1 and E2 versus time. To avoid the spurious contribution of low disperse magnetic flux, for the computation we only considered magnetic strengths above 200 G. It can be noticed that although fluxes are relatively comparable, bipoles E1 and E2 seem to have different magnetic flux evolutions. Bipole E1 is the first one to emerge and reaches its maximum flux by mid March 16, while E2 begins its emergence later and continues to increase its flux until March 18. It is also worth noting that the flux of both polarities within each bipole evolve in a consistent manner.

There is no available vector magnetogram data for the full evolution of this AR. Only a single vector magnetogram from the Mees Observatory Imaging Vector Magnetograph (MSO/IVM) was obtained on March 18. Although due to projection effects this magnetogram is not recommended for quantitative analysis (the AR is located at W45 on March 18), visual inspection of the direction of the transverse field indicates a strong shear close and around the polarity inversion line of the δ-spot. As we describe in the following sections, this magnetic shear has important consequences in relation with the high level of activity observed in the region, and also with our interpretation of the magnetic structure of the flux tube that gave origin to the AR.

2.2. AR 10314 coronal structure and activity

To study the coronal structure and evolution of AR10314 we used a set of 773 images obtained in the 195Åband with the Extreme Ultraviolet Imaging Telescope (EIT, Delaboudinière et al., 1995) on board SOHO. In Fig. 3 we show selected EIT images. In the upper panels, corresponding to March 14 and 15, it is possible to identify the two main arcades that connect the polarities of bipoles E1 and E2 (see Fig. 1). As the polarities of the δ-spot rotate one around the other during March 16 and 17 (Fig. 3, middle panels) the coronal structure of the AR becomes more complex. As a consequence of the increasing complexity and the related magnetic energy accumulation, by the end of March 17 the AR begins to produce a series of major flares that continue during the following 2 or 3 days. A total of 37 flares have been identify as being produced by this AR. In Table 1 we present a list of the flares with their corresponding durations and GOES (Geostationary Operational Environmental Satellite) X-ray classification obtained from Solar Geophysical Data. In that period 2 X-class flares and 7 M-class flares occurred in the region.

In Fig. 4 we plot the EUV flux of AR 10314 versus time computed from the set of EIT images. We indicate with labels the 4 most energetic flares produced by the AR. The identification was made comparing the times of the EUV peaks with X-ray data from GOES. It is noticeable the change of slope of the lightcurve around the last third of March 17, that is almost coincident with the occurrence of the first X class flare produced by the AR.

During the major flares a complete restructuring of the coronal organization can be observed. The lower panels of Fig. 3 correspond to EUV images of the AR taken a few hours, respectively, before and after the X1.5 flare that occurred around 12:00UT on March 18. Before the flare the coronal configuration is clearly sigmoidal with a remarkable shear in the area coinciding with the inversion line of the δ-spot. As we describe in the previous section, vector magnetogram data also show a pronounced magnetic shear

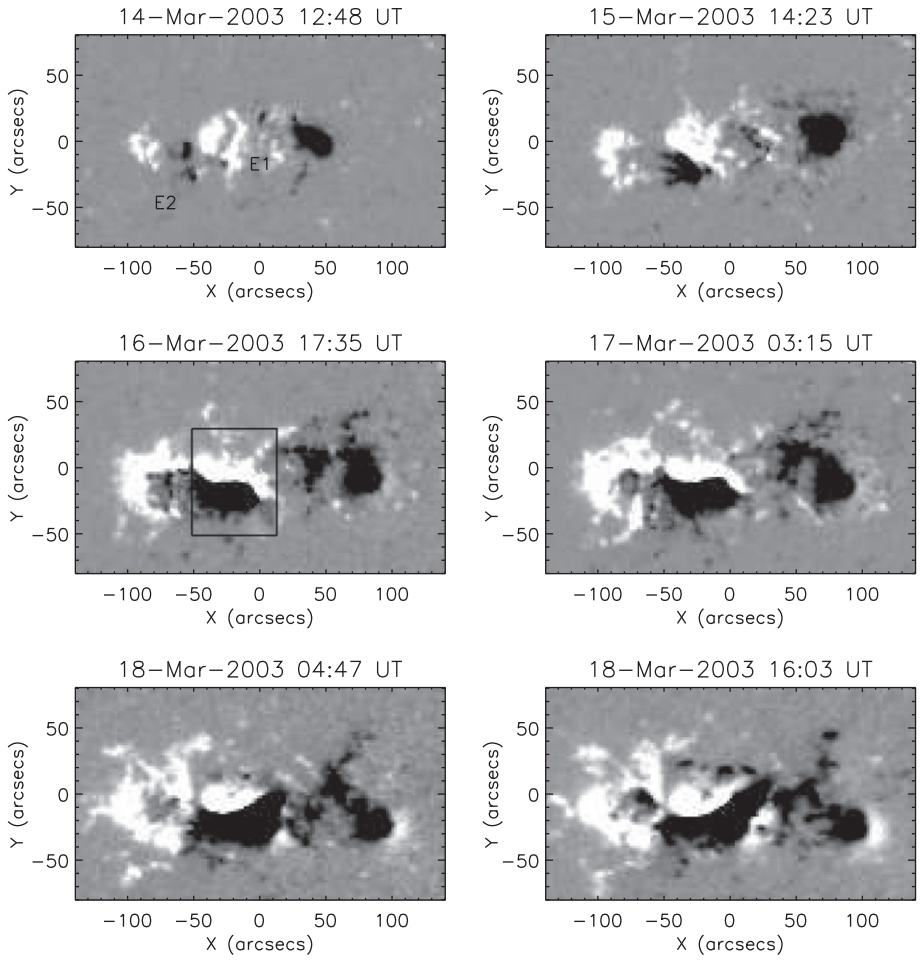

Fig. 1. Selected SOHO/MDI magnetograms for the evolution AR 10314. The AR was observed from its first emergence on March 13, 2003 to its disappearance on the west limb around March 20, 2003. In the upper left panel we identify the emergence of the two main bipoles (E1 and E2) that form the quadrupolar structure of the AR. In the middle left panel we indicate with a square the location of the δ-spot formed at the center of the AR. The opposite polarities of the δ-spot are observed to rotate one around the other during the studied evolution.

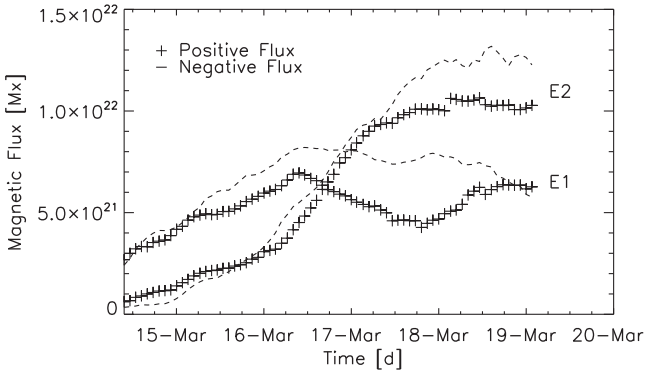

Fig. 2. Magnetic flux evolution of the 4 main polarities that form the quadrupolar structure of AR 10314. We group the polarities in bipoles E1 and E2 as shown in Fig. 1. Bipole E1 emerges first and reaches its maximum flux by mid March 16. Bipole E2 continues to emerge reaching a higher maximum flux by March 18.

in the proximities of the inversion line. After the flare (see Fig. 3, lower right panel) the loop configuration is more potential, indicating a relaxation of the magnetic stress present in the region before the event. This reconfiguration of the coronal magnetic structure is usually observed in ARs producing major flares (Benz, 2008). In Section 4 we discuss and interpret the peculiar evolution of AR 10314 and relate it with the observed high level of activity.

3. Analysis

3.1. Evolution of the δ-spot tilt

As described in Section 2.1, the δ-spot that forms in the center of AR 10314 by the apparent coalescence of polarities from bipoles E1 and E2 has a fast and continuous rotation during most of the AR evolution. In order to compute this rotation quantitatively we define the tilt of the magnetic configuration as the vector joining the mean flux centers of the positive and negative polarities that form the δ-spot. We determine the position of the positive (+) and negative (−) flux centers using:

$$X_{\pm} = \frac{\sum xB_{\pm}}{\sum B_{\pm}}, \quad Y_{\pm} = \frac{\sum yB_{\pm}}{\sum B_{\pm}}, \tag{1}$$

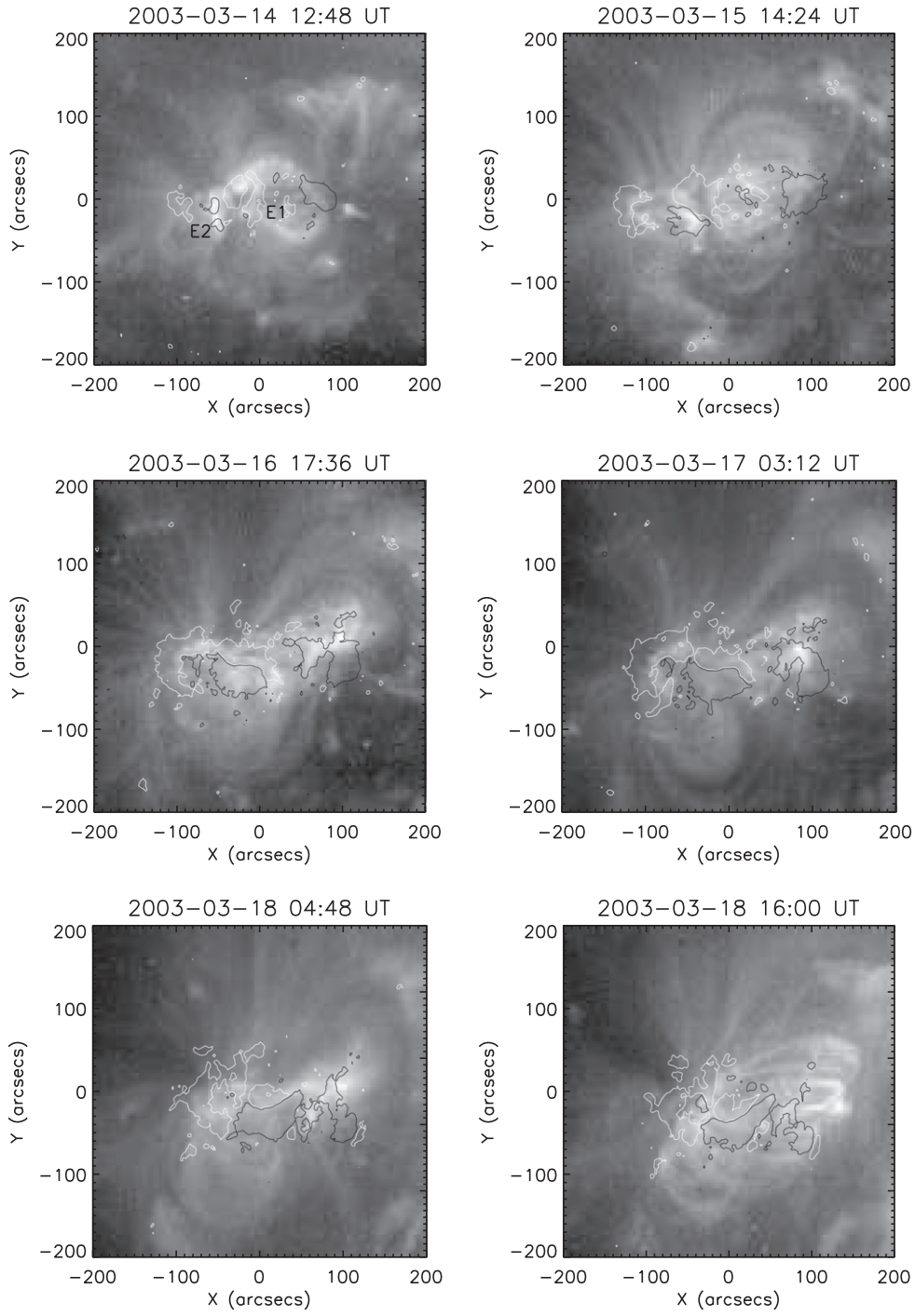

Fig. 3. Evolution of the coronal structure of AR 10314 observed in SOHO/EIT images obtained in the 195 Åband. Overlayed white and black contours correspond to positive and negative photospheric magnetic fields of 200 G strength. These images show how the complex evolution of the AR magnetic distribution determines the coronal configuration. In the two lower panels it can be appreciated the change in the coronal structure before and after one of the major flares produced in the AR (see Section 2.2).

where x and y are the coordinates of each pixel on the magnetogram and B is the corresponding normal magnetic field component (computed from the longitudinal component supposing that the photospheric magnetic field is radial). For the sum, only magnetic field strengths above a chosen threshold are considered. From the above expression we can compute the module of the tilt vector using:

$$S = \sqrt{(X_- - X_+)^2 + (Y_- - Y_+)^2}, \tag{2}$$

and the tilt angle with respect to the east–west direction as:

$$\psi = arctan\frac{(Y_- - Y_+)}{(X_- - X_+)}. \tag{3}$$

Table 1
List of flares produced by AR 10314. The indicated times correspond to the peaks of X-ray emission. Data obtained from GOES observations and *Solar Geophysical Data*.

Date and time (UT)	Duration (min)	X-ray class (GOES)	Date and time (UT)	Duration (min)	X-ray class (GOES)
15-Mar 03:36	35	B8.1	18-Mar 12:08	344	X1.5
15-Mar 15:30	50	C3.7	18-Mar 16:20	44	C2.8
15-Mar 20:16	82	C8.4	18-Mar 19:03	78	C5.9
16-Mar 04:15	115	C3.0	18-Mar 23:28	111	C5.1
16-Mar 11:29	35	C1.0	19-Mar 02:44	38	C3.4
16-Mar 13:12	34	C1.2	19-Mar 03:07	238	M1.5
16-Mar 21:35	129	C1.1	19-Mar 06:46	92	M1.6
17-Mar 01:03	60	C3.1	19-Mar 09:53	70	M3.7
17-Mar 02:47	55	B9.1	19-Mar 11:25	23	C5.8
17-Mar 16:50	86	C7.7	19-Mar 13:32	26	M1.4
17-Mar 19:05	356	X1.5	19-Mar 16:48	49	C3.2
17-Mar 20:21	73	C6.9	19-Mar 18:54	40	C6.3
18-Mar 00:37	67	M1.6	19-Mar 21:04	25	C1.8
18-Mar 01:53	95	C4.7	19-Mar 21:28	39	C2.2
18-Mar 04:05	153	C7.5	19-Mar 22:00	13	C3.5
18-Mar 06:00	37	M2.5	19-Mar 23:15	28	C2.0
18-Mar 06:45	69	C2.1	20-Mar 02:31	42	C9.1
18-Mar 07:42	97	C2.8	20-Mar 11:31	97	M1.5
18-Mar 10:23	87	C2.4			

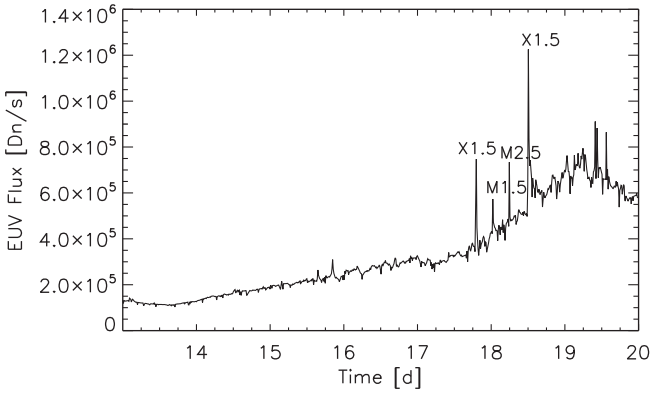

Fig. 4. EUV flux versus time obtained from the set of SOHO/EIT images in the 195Åband used to study the coronal evolution of AR 10314. The sudden increases of intensity due to the 4 major flares produced in the AR are identified with labels.

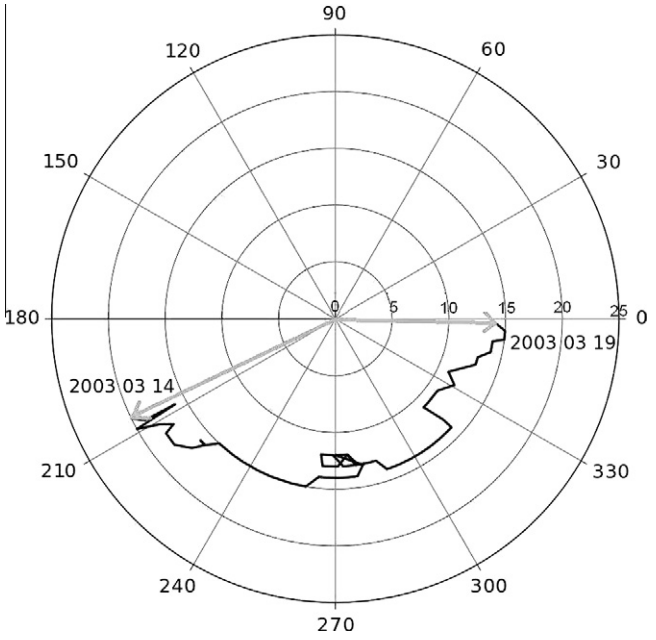

Fig. 5. Polar plot showing the evolution of the tilt vector of the δ-spot. The center of the plot corresponds to the position of the center of positive polarity and the black line indicates the relative position of the negative one. Therefore, the radial coordinate corresponds to the module of the tilt vector S computed according to Eq. (2), and the angular coordinate represents the tilt angle ψ defined by Eq. (3). The arrows represent the tilt vector for the initial and final dates of the studied data set. Radial units are in Mm.

In the polar plot of Fig. 5 we show the evolution of the δ-spot tilt computed from SOHO/MDI magnetograms. The center of the plot corresponds to the position of the positive polarity, while the head of the arrows and the line indicate the relative position of the negative one. For clarity, we only draw arrows for the initial and final dates. With the chosen convention, the direction of the tilt vector coincides with the local orientation of the magnetic field. The results shown in Fig. 5 clearly confirm the pronounced counter-clockwise rotation of the δ-spot region observed by visual inspection of the magnetograms. The total rotation of the tilt angle obtained from the computations is approximately 150 deg. This correspond to an approximate mean angular velocity of 30 deg/day. Although the rotation is continuous during most of the observed evolution, there is a small backward motion around the beginning of March 17. This apparent short-term counter-rotation is due to a brief new flux emergence in the eastern part of the δ-spot negative polarity.

In Fig. 5, one observes that the distance S between both polarity centers is roughly constant during the full evolution. As we discuss in Section 4 this suggests the

existence of a sub-photospheric magnetic link between the polarities of the δ configuration.

3.2. Magnetic helicity injection

In this Section we compute the magnetic helicity injected in AR 10314 during the studied evolution. To do so we use the Differential Affine Velocity Estimator (DAVE) method developed by Schuck (2005, 2006), (see also Démoulin and Pariat, 2009). The window size used was of 11 pixels ≈21 arcsec as suggested in the references. Basically, the procedure consists in the computation of the magnetic helicity injection rate given by the expression:

$$\frac{dH_r}{dt} = -\frac{1}{2\pi}\int_S\int_{S'}\frac{d\theta}{dt}B_n(\mathbf{r})B_n(\mathbf{r}')dSdS' \quad (4)$$

where H_r is the relative magnetic helicity with respect to the potential field (Berger and Field, 1984) and $\frac{d\theta}{dt}$ is the rate of mutual rotation between features at locations r and r' having magnetic strengths $B_h(r)$ and $B_h(r')$, respectively. The velocities used to obtain $\frac{d\theta}{dt}$ are determined using a LCT technique. We use a numerical code that computes from the studied SOHO/MDI magnetograms the magnetic helicity density defined by:

$$G_\theta(\mathbf{r}) = -\frac{B_n(\mathbf{r})}{2\pi}\int_{S'}\frac{d\theta(\mathbf{r}-\mathbf{r}')}{dt}B_n(\mathbf{r}')dS'. \quad (5)$$

The helicity density maps obtained from the above procedure show that, although there are contributions of both signs of helicity in different areas of the AR, there is a clear predominance of positive sign helicity. Analyzing the distribution of the magnetic helicity density throughout the AR we find that most of the positive injection is due to the rotation of the δ-spot.

In Fig. 6 upper panel we plot the total magnetic helicity flux versus time obtained integrating the helicity injection density in the whole AR. The positive and negative helicity contributions are plotted with dashed lines and the continuous line corresponds to the total injection. The plot confirms the positive helicity predominance. It is noticeable not only the marked fluctuations of the positive component with respect to the negative, but also the presence of a sudden decrease of the positive injection by the beginning of March 17, followed by a rapid increase in the following few hours. Visually inspecting the MDI magnetograms for the corresponding date and times we found that there is a small area within the negative polarity of the δ-spot where pixels have abnormally low field values. We think that these pixels have wrong values possibly due to the high field strength associated to the δ region. The reason why these defective pixels affect the computation of the helicity injection rate can be understood from Eq. (5). There, it can be seen that the injection depends on both the rate of rotation between features and their corresponding magnetic strengths. Therefore, the sudden appearance of low field pixels in locations where high magnetic strength was present artificially decreases the computed magnetic helicity flux.

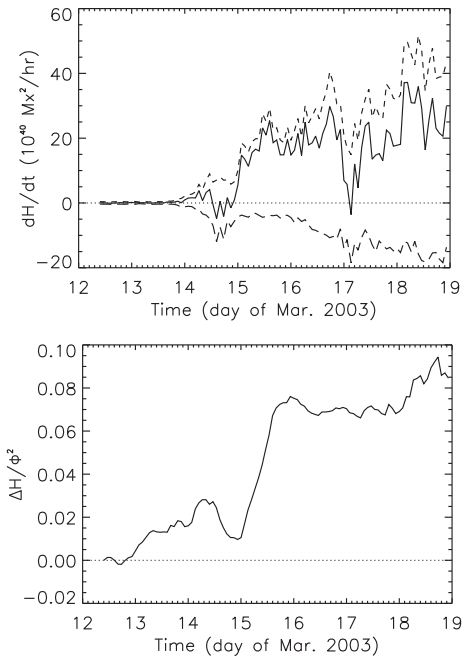

Fig. 6. Upper panel: rate of magnetic helicity injection in function of time computed using the technique described in Section 3.2. Broken lines correspond to positive and negative helicity contributions and the solid line indicates the net injected helicity. The origin of the sudden decrease in the positive helicity injection observed on the beginning of March 17 is explained in Section 3.2. Lower panel: ratio of the total accumulated helicity to the square of the AR magnetic flux versus time. Both plots indicate a clear predominance of positive helicity injection.

We integrate the injection rate computed above to obtain the accumulated magnetic helicity in function of time. In the lower panel of Fig. 6 we plot the evolution of the accumulated helicity divided the square of the total unsigned flux of the AR. The curve further confirms the overwhelming predominance of positive magnetic helicity in AR 10314. The ratio of the accumulated helicity to the square of the AR flux is within the range obtained by (Démoulin and Pariat (2009), see their Section 3.2.3). The total accumulated helicity by the end of the analyzed evolution is 21×10^{42} Mx^2, which is comparable to values from similar ARs studied in previous works (see e.g. Tian and Alexander, 2008).

As it is the case in other very complex ARs, the high magnetic helicity flux is related to the high level of activity produced by the AR. The influx of magnetic helicity driven by photospheric motions and the emergence of twisted magnetic fields imply the accumulation of free magnetic energy that is eventually released during flares and CMEs. In the next Section, we propose an interpretation of the described evolution in terms of the emergence of a deformed magnetic flux tube.

4. Discussion

The results described in the previous sections allow us to infer a possible structure for the magnetic flux tube that gave origin to AR 10314. In Fig. 7 we show a drawing of

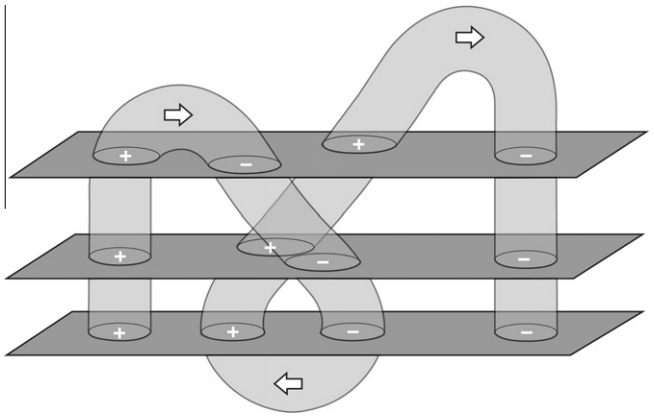

Fig. 7. Inferred structure of the magnetic flux tube that produced AR 10314. The planes indicate the relative position of the photosphere during the flux tube emergence, the arrows show the global direction of the magnetic field along the tube, and the circles with signs correspond to the location of the polarities observed at the photospheric plane for different stages of the evolution.

the proposed flux tube configuration, consisting in a Ω loop whose top has been bended and curled downwards. In the figure the arrows indicate the main direction of the flux tube magnetic field, the planes correspond to the relative position of the photosphere during the emergence (the evolution of the photospheric plane must be followed from top to bottom), and the circles with pluses and minuses represent the polarities and their corresponding signs at photospheric level. In what follows we discuss the arguments that led us to conclude the consistency of the scheme shown in Fig. 7 with the observed AR characteristics and evolution.

The main bipoles that form the AR emerge almost simultaneously. Although there is a possibility that the bipoles are due to two independent flux tubes emerging together (e.g. if they belong to the same flux nest, see Gaizauskas, 2008), the coincidence in time suggests the presence of a single global structure. It is worth to note that the evolution of the bipoles magnetic fluxes are somewhat different, E2 reaches a higher maximum than E1. This could be an argument in favor of independent magnetic flux tubes, however, since E1 emerges before E2, it is possible that by the time their fluxes are similar E2 begins to disperse resulting in an underestimation of the computed flux. In the scheme proposed in Fig. 7 the delay between the emergence of bipoles E1 and E2 is explained considering that one of the flux tube "tops" is higher than the other, and therefore crosses the photosphere first.

As we began to discuss in Section 3.1, the evolution of the tilt vector is consistent with the presence of a strong subphotospheric link between the two polarities of the δ-spot. The distance between the main polarity centers remains approximately constant during the full observed evolution, demonstrating that both polarities are actually rotating one around the other. The persistence of both polarities to remain packed together strongly suggest that they belong to the same structure. This behavior would not be expected in the case of polarities produced by independent flux tubes. It is also worth to mention that the observed rotation is much higher and opposes the expected relative motion produced by solar differential rotation. The AR is in the south hemisphere, so if the rotation was just due to differential rotation one would expect the northern polarity of the δ region to travel faster to the west than the southern one, not the opposite case, as it is observed. The persistence of the δ configuration during the evolution of the AR and the observed fast rate of rotation are strong arguments in favor of a single magnetic flux system.

It is expected that the configuration proposed in Fig. 7 produces a particular magnetic geometry at and around the inversion line of the δ-spot. To be consistent with the global structure, magnetic field lines right above the inversion line should have their concavity facing upwards, forming what is known as bald patches (Bungey et al., 1996) at the photospheric level. This kind of magnetic field distribution is propitious for the formation of a filament above the inversion line. We analyze a set of Hα images obtained with the Hα Solar Telescope for Argentina (HASTA) for the studied dates and we confirm the presence of a filament in that location. A further support for the described local magnetic geometry could be determined from the analysis of vector magnetogram data. As we discussed in Section 2.1 we could only obtain one vector magnetogram from MSO/IVM for March 18. Unfortunately, in that date the region was too far from central meridian and projection effects make the quality of the data insufficient for a detailed analysis of the local magnetic structure. However, as we state in Section 2.1, the vector magnetogram data show a strong shear in and around the inversion line. The magnetic field deformation associated to the observed shear is consistent with the injected positive helicity computed in Section 3.2. The presence of shear in the vicinity of the neutral line indicates the accumulation of free magnetic energy in the AR and is a very well known precursor of strong flaring activity.

If it was possible to observe the long term evolution of AR 10314, the continuous emergence followed by photospheric dispersion would clearly produce different patterns in the cases of single versus double flux tube configurations discussed above. After the decay phase, two independent magnetic flux tubes are expected to evolve to form two identifiable extended bipoles at the photospheric level, while a single flux tube would eventually appear as a single extended bipole. Although the photospheric magnetic appearance of AR 10314 becomes unobservable around March 20 when it reaches the west solar limb, we studied MDI magnetograms corresponding to the expected location of the region in the next solar rotation. Visual inspection of these magnetograms show a single extended bipole as it would be the case of the evolved state of a single magnetic flux tube. The presence of this flux configuration at the expected location of the AR is another argument in favor of a single distorted magnetic flux tube.

The magnetic helicity of a flux tube, as the one represented in Fig. 7, can be separated in two components. The so called twist is the helicity due to the rotation of the magnetic field lines around the main axis of the tube, while the deformation of the axis (the flux tube as a whole) is called writhe. According to the scheme shown in Fig. 7 the sign of writhe for the proposed structure is positive (the deformation follows the rule of the right hand). As we described in Section 3.2 the helicity injected in the AR during the analyzed evolution has an overwhelming predominance of positive sign. The fact that both twist and writhe have the same sign suggests a particular physical mechanism as the origin of the flux tube deformation. It has been proposed that δ-spots could be the manifestation of the emergence of magnetic flux tubes that have been deformed by the development of a kink instability (see e.g. Fan et al., 1999). Since the kink instability implies an internal transfer of magnetic helicity from twist to writhe, the theory predicts that kinked flux tubes must have the same sign for both helicity components. Considering the magnetic helicity computed in Section 3.2 and assuming the tube structure presented in Fig. 7, the case studied here is consistent with this kind of mechanism. It is worth to note however, that other processes, such as the interaction of the flux tube with external plasma motions during its emergence through the convective zone cannot be ruled out as the cause of the inferred deformation (see López Fuentes et al., 2003).

5. Conclusions

We studied the photospheric and coronal evolution of AR NOAA 10314 using SOHO/MDI and EIT observations. This AR was characterized for being particularly active, producing two X-class flares and several less energetic events during a few days. From our analysis we conclude that the origin of the observed high level of activity is the fast accumulation of free magnetic energy that is injected into the corona during the emergence of the severely twisted and writhed magnetic flux tube that forms the AR. The computation of the tilt vector and the magnetic helicity show that the injected helicity is of positive sign and is mainly produced by the fast rotation of the δ-spot at the center of the magnetic configuration. From our results we propose a possible morphology for the magnetic flux tube that gave origin to AR 10314 and discuss the plausibility of the kink instability as the physical mechanisms behind the inferred deformation.

Acknowledgements

The authors would like to thank Dr Manolis Georgoulis for providing processed MSO/VMI data used in this work and Dr. Peter Schuck for the permission to use the Differential Affine Velocity Estimator (DAVE) routine. SOHO is a project of international cooperation between ESA and NASA. MP, MLF, and CHM acknowledge financial support from the Argentinean grants PICT 2007-1790 (ANPCyT), UBACyT 20020100100733 and PIP 2009-100766 (CONICET). MLF and CHM are members of the Carrera del Investigador Científico (CONICET). This work was developed in the frame of the ECOS-MinCyT agreement (No. A08U01) between collaborating solar physics groups from France and Argentina.

References

Benz, A.O. Flare observations. Living Rev. Solar Phys. 5, 1, 2008.
Berger, M.A., Field, G.B. The topological properties of magnetic helicity. J. Fluid Mech. 147, 133–148, 1984.
Bungey, T.N., Titov, V.S., Priest, E.R. Basic topological elements of coronal magnetic fields. Astron. Astrophys. 308, 233–247, 1996.
Delaboudinière, J.-P., Artzner, G.E., Brunaud, J., et al. EIT: Extreme-Ultraviolet Imaging Telescope for the SOHO mission. Sol. Phys. 162, 291–312, 1995.
Démoulin, P., Pariat, E. Modelling and observations of photospheric magnetic helicity. Adv. Space Res. 43, 1013–1031, 2009.
D'Silva, S., Choudhuri, A.R. A theoretical model for tilts of bipolar magnetic regions. Astron. Astrophys. 272, 621–633, 1993.
Fan, Y. Magnetic fields in the solar convection zone. Living Rev. Solar Phys. 6, 4, 2009.
Fan, Y., Zweibel, E.G., Linton, M.G., Fisher, G.H. The rise of kink-unstable magnetic flux tubes and the origin of delta-configuration sunspots. Astrophys. J. 521, 460–477, 1999.
Gaizauskas, V. Development of flux imbalances in solar activity nests and the evolution of filament channels. Astrophys. J. 686, 1432–1446, 2008.
Hale, G.E., Ellerman, F., Nicholson, S.B., Joy, A.H. The magnetic polarity of sun-spots. Astrophys. J. 49, 153–185, 1919.
Hale, G.E., Nicholson, S.B. Magnetic observations of sunspots, 1917–1924. Washington, D.C. Carnegie institution of Washington, 1938.
Liu, C., Deng, N., Liu, Y., et al. Rapid change of δ-spot structure associated with seven major flares. Astrophys. J. 622, 722–736, 2005.
Longcope, D., Choudhuri, A.R. The orientational relaxation of bipolar active regions. Sol. Phys. 205, 63–92, 2002.
López Fuentes, M.C., Démoulin, P., Mandrini, C.H., Pevtsov, A.A., van Driel-Gesztelyi, L. Magnetic twist and writhe of active regions. On the origin of deformed flux tubes. Astron. Astrophys. 397, 305–318, 2003.
Morita, S., McIntosh, S.W. Genesis of AR NOAA10314, in: Sankarasubramanian, K., Penn, M., Pevtsov, A. (Eds.), ASP Conference Series, vol. 346, pp. 317–325, 2005.
Scherrer, P.H., Bogart, R.S., Bush, R.I., et al. The solar oscillations investigation – Michelson Doppler Imager. Sol. Phys. 162, 129–188, 1995.
Schrijver, C.J., Zwaan, C. Solar and stellar magnetic activity. Cambridge Astrophys. Ser., 34, 2000.
Schuck, P.W. Local correlation tracking and the magnetic induction equation. Astrophys. J. Lett. 632, L53–L56, 2005.
Schuck, P.W. Tracking magnetic footpoints with the magnetic induction equation. Astrophys. J. 646, 1358–1391, 2006.
Tian, L., Alexander, D. On the origin of magnetic helicity in the solar corona. Astrophys. J. 673, 532–543, 2008.